JOURNAL OF PROPULSION AND POWER
Vol. 19, No. 4, July–August 2003

Constant-Frequency Hypervelocity Slings

D. A. Tidman*
Advanced Launch Corporation, McLean, Virginia 22101-1576

The dynamics of projectile acceleration in a slingatron ring that gyrates with a constant frequency is analyzed, assuming that projectile sliding friction forces are negligible. It is found that projectiles injected into the ring can accelerate for several turns around the ring to very high velocity, but must then exit before they start to decelerate. The interaction can be formulated as a "soft elastic collision" between the projectile and the track displacement wave that travels at high speed around the orbiting ring. Projectiles execute a swing in phase relative to the traveling wave as they accelerate and are thrown forward. The diameter of the slingatron in this case is smaller than for a slingatron designed for phase-locked acceleration to the same velocity. This same phase swing approach could be used to reduce the size of both ring and spiral slingatron mass accelerators. A multiturn spiral machine with close turns approximates a ring and appears capable of launching a stream of projectiles to high velocity. Scaling arguments indicate that both the friction coefficient and the fraction of projectile mass lost in sliding to a given velocity become smaller for larger projectiles.

Nomenclature

A	=	contact area of projectile bearing on track resolved perpendicular to R
$F_\perp$	=	centripetal force of track on projectile
f	=	orbiting frequency of ring, cps
L_{arm}	=	total length of swing arm including load and counterweight sides
m	=	projectile mass
N_{turns}	=	number of projectile transits around ring to reach maximum speed
n_{pairs}	=	number of swing arm pairs distributed along spiral
P	=	average pressure of gas in projectile bearing
R	=	radius of curvature of the track in the launch tube ring
R_1, R_2, R_3,etc.	=	radius of curvature of successive semicircles for spiral construction
r	=	swing radius of ring orbital motion
T	=	dimensionless time as number of gyration periods, ft
t	=	time
V	=	projectile speed relative to track
V_{exit}	=	speed of projectile relative to track at exit
V_{lab}	=	projectile speed in laboratory frame
V_{wave}	=	speed of displacement wave traveling around ring, Rv/r
V_0	=	injection speed of projectile relative to track
v	=	swing speed of ring in laboratory frame
x, y	=	coordinate axes in laboratory frame
y_{film}	=	thickness of projectile gas bearing film
α	=	ring radius divided by swing radius, R/r
β	=	multiplier for scaling dimensions to a geometrically similar sling
ΔV	=	average gain in projectile speed per turn in accelerating through the sling
η_{visc}	=	viscosity of gas in projectile bearing
θ	=	angle between swing velocity v and projectile velocity V
$\theta_{\max}$	=	maximum value of θ during projectile collision with wave
μ_{roll}	=	rolling friction coefficient of bearings
μ_{slide}	=	sliding friction coefficient of projectile
τ_{scatt}	=	angular scattering time averaged over atoms and molecules in bearing gas
ϕ	=	phase angle of projectile position around ring
ψ	=	gyration phase angle of ring in laboratory frame

Received 3 December 2002; accepted for publication 28 March 2003.

*President, 6801 Benjamin Street. Senior Member AIAA.

Introduction

THE slingatron mass accelerator is a device that implements the simple principles found in the ancient sling. Unlike the ancient sling, it appears capable of launching a stream of projectiles with extremely high velocity. Spiral and circular versions of this machine have been discussed.[1–9] Here we discuss the dynamics of constant-frequency circular machines and spirals with close turns because these are relatively simple to construct and cover a wide range of interest for applications. Data on the passage of fast projectiles through curved tubes, along with potential applications, have been discussed earlier.[6]

Figure 1 shows an example in which the guide tube is formed as a two-turn spiral with close turns. The accelerator tube is mounted on swing arms distributed along the spiral so that it can be powered to execute a constant-frequency high-speed orbital motion, that is, the entire tube swings around a small circle of radius r without changing its orientation. The accelerator is contained in a housing (not shown) that could be evacuated to reduce air drag (if needed) on the high-speed orbital motion of the launch tube. The acceleration is similar to rolling a ball bearing around in a frying pan in a horizontal plane and gyrating the pan around a small circle, except that the gyration speed in this version of a sling is much higher and the projectile slides around the spiral turns on its self-generated gas film.

Projectiles accelerate around the spiral launch tube in the same clockwise sense as the rotation of the swing arms. A projectile can be either injected into the tube entrance, or can be released from an anchored position in front of a blocked breech.

The arm pairs shown in Fig. 1 have center spindles. They also have counterweights at one end of the arm that balance each arm's share of the centrifugal force of the orbiting tube and structure at the opposite end. The side load forces on the center spindle bearings are, thus, relatively small. The most stressed bearings are those at the tube end of the swing arms, where the side loads on the bearings must support the centrifugal force of the orbiting structure. However, this force is shared by distributing closely packed arms along the spiral, and by using two radial load needle bearings stacked in the cylindrical housing in the top and bottom swing arms, for a total of four bearings per arm pair. The load capacity could also be increased by radial nesting of bearings.

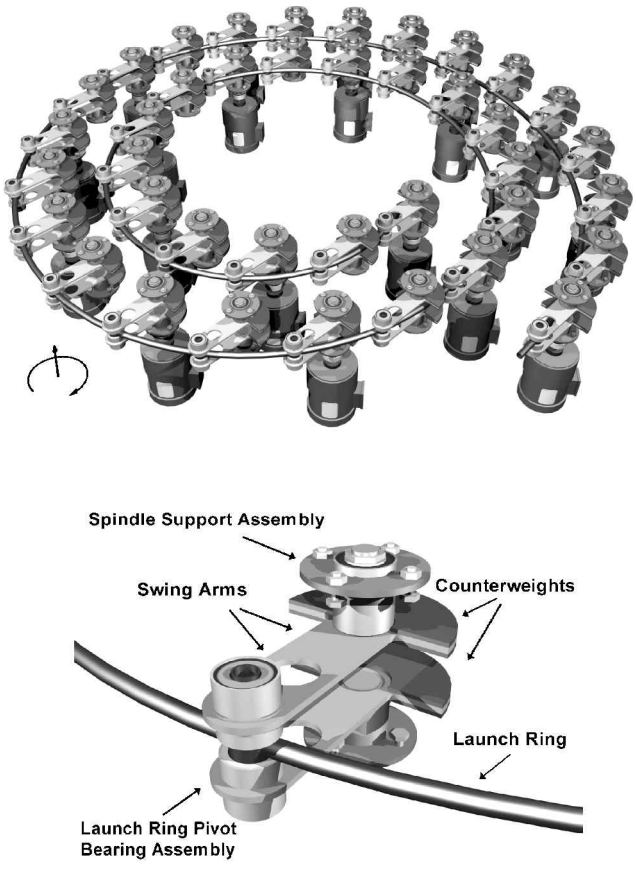

Fig. 1 Conceptual machine showing swing arm pairs distributed around a two-turn spiral sling.

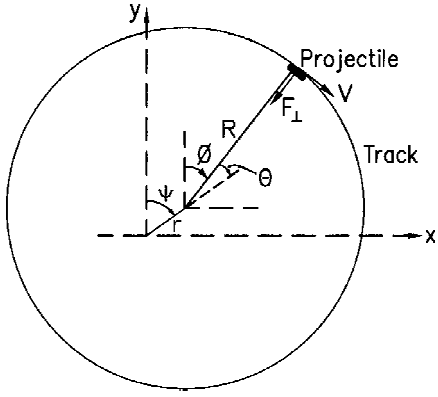

Fig. 2 Coordinate system with ring track radius R where projectile of mass m travels with speed V relative to the tube; entire tube orbits around its gyration circle of radius r with speed v in the laboratory x–y frame without changing its orientation.

There are two kinds of friction involved in this mass launcher, namely, the rolling friction of the sling bearings just described and the sliding friction of the projectile as it slides on its evaporated bearing film of hot gas. Both of these friction coefficients appear to decrease for mass launchers of increasing size, so that the approximation $\mu_{\text{slide}} = 0$ used later may become more useful for large projectiles.

Equations of Motion for a Frictionless Projectile Sliding in a Ring Slingatron Tube Gyrating at Constant Frequency

Figure 2 shows a projectile of mass m sliding in a circular guide tube. For simplicity we assume that the projectile sliding friction is zero, so that there is no force component acting on the projectile parallel to the track. Sliding friction has been discussed in earlier publications.[2,6] In addition, the angular speed $\dot{\psi}$ is assumed constant ($\ddot{\psi} = 0$). The equations of motion for the projectile located at (x, y) in Fig. 2 then become,

$$m\ddot{x} = -F_{\perp}\sin\phi, \qquad m\ddot{y} = -F_{\perp}\cos\phi \tag{1}$$

Assuming the projectile is constrained to slide in the circular track, we also have

$$x = r\sin\psi + R\sin\phi, \qquad y = r\cos\psi + R\cos\phi \tag{2}$$

When Eqs. (1) and (2) are combined , it follows that

$$R\ddot{\phi} = r\dot{\psi}^2\sin(\psi - \phi) \tag{3}$$

The projectile speed in the laboratory frame is

$$V_{\text{lab}} = \{R^2\dot{\phi}^2 + r^2\dot{\psi}^2 + 2rR\dot{\phi}\dot{\psi}\cos(\psi - \phi)\}^{0.5} \tag{4}$$

and the projectile speed V relative to the track and the ring orbiting speed v are

$$V = R\dot{\phi}, \qquad v = r\dot{\psi} = 2\pi rf \tag{5}$$

Dimensionless Parameters

Assume the circular guide tube is propelled by swing arms around its gyration circle of radius r at a constant frequency f (cycles per second) and constant gyration speed $v = 2\pi rf$. The gyration phase angle is, thus, $\psi = 2\pi ft$. We express Eq. (3) in terms of a dimensionless time variable $T = ft$ so that T is the number of elapsed periods. Equation (3) then becomes

$$\frac{\partial^2\theta}{\partial T^2} + \frac{(2\pi)^2}{\alpha}\sin\theta = 0, \qquad \theta = \psi - \phi = 2\pi T - \phi \tag{6}$$

where we also expressed Eq. (6) in terms of the dependent variable θ (Fig. 2), that is, the angle between the gyration velocity vector $\boldsymbol{v}$ and projectile velocity $\boldsymbol{V}$. Note that Eq. (6) is also the equation for a nonlinear pendulum.

The dimensionless variables are

$$T = ft, \qquad \alpha = R/r \tag{7}$$

and chosen initial values

$$\phi(T=0) = -\theta(T=0) = 0, \qquad V(T=0) = V_0$$

$$\left(\frac{\partial\theta}{\partial T}\right)_{T=0} = 2\pi - \left(\frac{\partial\phi}{\partial T}\right)_{T=0} = 2\pi - \frac{2\pi}{\alpha}\left(\frac{V_0}{v}\right) \tag{8}$$

Note that V_0 is the initial projectile velocity relative to the tube (inside the tube entrance) at $T = 0$. Making use of Eq. (5) and the second part of Eq. (6) also gives a useful relation

$$\frac{\partial\theta}{\partial T} = 2\pi\left(1 - \frac{V}{\alpha v}\right) \tag{9}$$

Traveling Potential Wave Model

Multiplying Eq. (6) by $\partial\theta/\partial T$, one can integrate and use the initial values (8) to obtain the constant of integration. This gives

$$\frac{1}{2}\left(\frac{\partial\theta}{\partial T}\right)^2 + \frac{(2\pi)^2}{\alpha}(1 - \cos\theta) = \frac{(2\pi)^2}{2}\left\{1 - \frac{V_0}{\alpha v}\right\}^2 \tag{10}$$

Because the projectile motion is frictionless, we see that its acceleration can be viewed as due to the elastic collision of a traveling potential wave with the projectile. The two terms on the left of Eq. (10) are analogous to the kinetic and potential energies. Equation (10) can also be rewritten using Eq. (9) to substitute for $\partial\theta/\partial T$, namely,

$$(1 - V/\alpha v)^2 + (2/\alpha)(1 - \cos\theta) = (1 - V_0/\alpha v)^2 \tag{11}$$

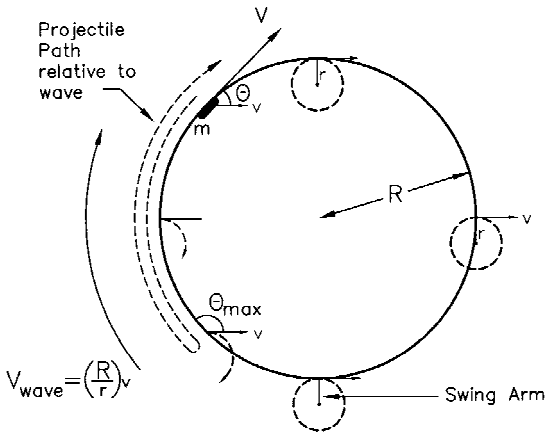

Fig. 3 Displacement wave of high speed Rv/r travels around the ring; projectile injected at $\theta = 0$ is overtaken by wave, so that $\theta > 0$, then accelerates back toward the wave front due to work done by the centripetal force.

This expresses the projectile velocity V as a function of its injection speed V_0, $\alpha = R/r$, the relative phase θ, and the swing speed v.

Figure 3 shows the path of a projectile (relative to the traveling wave) after injection with the chosen initial conditions (8). The gyration of the rigid ring with constant speed v around its orbiting circle of radius r causes a synchronous displacement of the entire ring that appears as a traveling displacement wave with speed $V_{\text{wave}} = \alpha v = Rv/r$. If the projectile injection speed is in the same clockwise sense but less than the wave speed, that is, $V_0 < V_{\text{wave}}$, the wave overtakes the projectile. However, the projectile can continue to accelerate for several cycles around the ring while in the relative phase range $\pi \geq \theta \geq 0$.

Next note that the projectile will have zero acceleration when the velocity vectors $\boldsymbol{v}$ and $\boldsymbol{V}$ are parallel, that is, $\theta = 0$ in Figs. 2 and 3, so that $\cos\theta = 1$. In this case, Eq. (11) yields two roots,

$$V = V_0, \qquad V = 2\alpha v - V_0 = 2V_{\text{wave}} - V_0 \tag{12}$$

The first root corresponds to the projectile initial speed V_0 at the wave front where $\theta = 0$, and the second root corresponds to the return of the projectile to the wave front at $\theta = 0$ after its initial fallback (relative to the wave) and later acceleration to a speed $V > V_{\text{wave}}$. This second root (12) corresponds to a two-body elastic collision in which the projectile is thrown forward by the wave traveling with speed $(R/r)v$ around the ring.

There is a minimum permissible initial speed V_0 for the projectile below which it will sink back relative to the overtaking wave and entirely penetrate the wave, that is, the projectile will not be thrown forward. To avoid penetration through the wave, we choose V_0 so that the projectile speed V equals the wave speed V_{wave} when it has penetrated to a maximum permissible relative phase $\theta_{\max}$. We will discuss a choice for $\theta_{\max}$ subsequently, but for the general result we substitute $V = \alpha v$ in Eq. (11) and solve for V_0 and use the resulting value of V_0 in Eq. (12) and find

$$V_0 = \left[\alpha - \sqrt{2\alpha(1 - \cos\theta_{\max})}\right]v$$

$$V_{\text{exit}} = \left[\alpha + \sqrt{2\alpha(1 - \cos\theta_{\max})}\right]v$$

$$\Delta V = 2v\sqrt{2\alpha(1 - \cos\theta_{\max})} \tag{13}$$

where V_{exit} is the projectile speed in the sling at exit and ΔV is the gain in projectile speed. We see that for large values of α the exit velocity becomes large because the projectile continues to accelerate while making several turns around the track circle. This occurs because the projectile interaction (as it first falls back and is then thrown forward by the wave) can involve an acceleration time of several gyration periods.

Note also that the projectile speeds [Eq. (13)] are relative to the tube at the projectile location. In the laboratory frame, the projectile initial speed for initial conditions (8) is $V_{0,\text{lab}} = V_0 + v$. A similar addition of v occurs at exit so that in the laboratory frame the exit speed is $V_{\text{exit}} + v$ because the exit is chosen to occur at the same phase $\theta = 0$. However, this zero relative phase with its maximum speed for exit will generally occur at a different physical location around the ring.

We next need an expression for the number of turns traveled around the ring by the projectile for a specific choice of α. This requires integration of Eq. (10). Substituting V_0 from Eq. (13) into Eq. (10) gives

$$\left(\frac{\partial\theta}{\partial T}\right) = \pm 2\pi\left(\frac{2}{\alpha}\right)^{\frac{1}{2}}(\cos\theta - \cos\theta_{\max})^{\frac{1}{2}} \tag{14}$$

The projectile velocity gain (13) involves an interaction time in which the projectile relative phase goes from $\theta = 0$ to $\theta_{\max}$ as it falls back into the wave and then from $\theta_{\max}$ to 0 as it accelerates back through the wave (like a surfer on an ocean wave). Because T can only increase, in integrating Eq. (14) we take the + root for the range 0–$\theta_{\max}$ and the − root for $\theta_{\max}$–0. The total dimensionless time taken for the projectile to accelerate to its maximum speed then follows from Eq. (14) as

$$T_{\text{exit}} = \frac{1}{\pi}\left(\frac{\alpha}{2}\right)^{0.5}\int_0^{\theta_{\max}} \frac{\mathrm{d}\theta}{\sqrt{\cos\theta - \cos\theta_{\max}}} \tag{15}$$

Furthermore, the number of turns N_{turns} traversed by the projectile equals its path length divided by $2\pi R$, and it follows from Eq. (9) that

$$N_{\text{turns}} = \frac{1}{2\pi R}\int_0^{T_{\text{exit}}} V\,\mathrm{dt} = T_{\text{exit}} \tag{16}$$

The integral (15) can be expressed in terms of an elliptic integral of the first kind, F,

$$\int \frac{\mathrm{d}x}{(a + b\cos x)^{\frac{1}{2}}} = \sqrt{\frac{2}{b}}F\left(\gamma, \frac{1}{\eta}\right), \qquad \eta = \left(\frac{2b}{a+b}\right)^{\frac{1}{2}}$$

$$\gamma = \sin^{-1}\left[\frac{b(1 - \cos x)}{a + b}\right]^{\frac{1}{2}} \tag{17}$$

(See Gradshteyn and Ryzhik[10] p. 154 for the result and p. 904 for the definition of F.) This is valid for $b \geq \text{modulus}\, a > 0$ and $0 \leq x < \cos^{-1}(-a/b)$. Using this formula with integrals (15) and (16) gives for the number of turns to maximum speed,

$$N_{\text{turns}} = \left(\sqrt{\alpha}/\pi\right)\{F[\pi/2, \sin(\theta_{\max}/2)] - F[0, \sin(\theta_{\max}/2)]\} \tag{18}$$

Close-Turns Spiral Machines

The preceding solutions include cases in which the projectile continues to accelerate for several turns around a circular track. There are various ways to design for projectile injection and its subsequent exit after a few transits around a single turn ring. However, here we consider a "close-turns spiral" design that approximates a ring for large $\alpha = R/r$ because this has a simpler entrance and exit than a ring, as shown in Figs. 1, 4, and 5. The spiral accelerator tube could, for example, be configured as a series of semicircles (Fig. 4) in which the semicircles have radii R_1, R_2, R_3, etc., with closely spaced alternate centers displaced by Δ. The centers and connections between the semicircles lie along a diameter as shown by the dotted line in Fig. 4. For this configuration, the projectile speed V is continuous in crossing from one semicircle to the next, but there is a jerk $\ddot{V}$ as the projectile centripetal acceleration $\dot{V}$ changes from V^2/R_n to V^2/R_{n+1}. This would cause only a small disturbance in

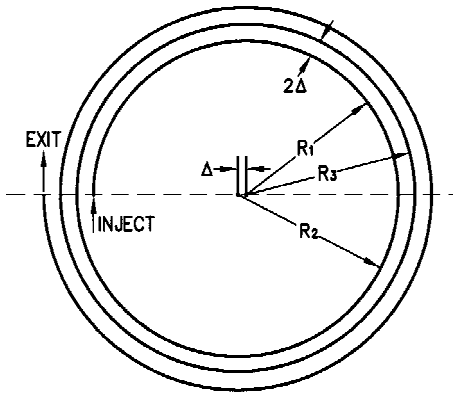

Fig. 4 Spiral constructed as a series of semicircles approximates ring for large R; spacing 2Δ between distributed arms chosen slightly larger than swing arm lengths.

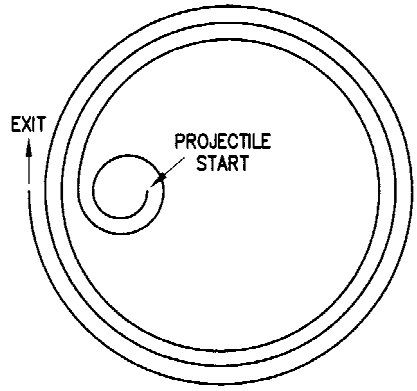

Fig. 5 Two-stage slingatron with small R inner stage that feeds into a large R outer spiral with three turns.

the projectile motion. Numerical solutions for spirals can be obtained using Eq. (6), except that the quantity $\alpha_n = R_n/r$ changes as the projectile crosses the series of semicircle boundaries,

$$R_1 = \alpha_1 r, \qquad 0 \le \phi \le \pi$$

$$R_2 = \alpha_2 r, \qquad \pi < \phi \le 2\pi$$

$$R_3 = \alpha_3 r, \qquad 2\pi < \phi \le 3\pi, \text{ etc.} \tag{19}$$

For large α, this design approximates the ring machine discussed in the preceding sections. The gap between neighboring turns, although small, must suffice for swing arms to be distributed along the entire spiral path without mutual collision. Close packing of the arms along the tube has the advantage that the load on the swing arm bearings can remain sufficiently below their rated loads so that the machine has a long lifetime. Furthermore, because the gap between turns is relatively small for example, $<2r$, one could distribute a few radial struts between turns to maintain its rigid structure. Struts could be located at one end of a few arm spindle shafts (not on the spiral tube) and orbit with frequency f around a radius less than r with a swing speed less than v. Synchronization of the swing arms could also be assisted by electronically synchronizing the drive motors.

Summary of Formulas and Examples

Equations (13) and (18) are the basic results for the family of ring slingatrons and also provide approximate results for spirals with closely spaced turns. We discuss some of the characteristics of these machines using a specific choice for $\theta_{\max}$ in the equations. First note that we cannot choose $\theta_{\max} = \pi$ for the maximum relative phase at the projectile reflection point in the wave (Fig. 3). This is because the integral (15) diverges for $\theta_{\max} = \pi$, as is also evident from Eq. (18) because $F(\pi/2, 1)$ is also infinite. The physical reason for this is that the projectile will spend an infinite time at the reflection point where it will ride along with the wave speed unless perturbed or experiencing sliding friction.

For an example we choose $\theta_{\max} = 0.75\pi$ for the projectile reflection point so that $\cos\theta_{\max} = -\sqrt{0.5}$. This leaves a margin for the neglected effect of sliding friction. In this case, Eqs. (13) and (18) give the injection and exit speeds V_0 and V_{exit}, of the projectile relative to the track, the number of turns it cycles around the ring, and the average velocity gain ΔV per cycle,

$$V_0/v \cong \alpha - 1.85\sqrt{\alpha}, \qquad V_{\text{exit}}/v \cong \alpha + 1.85\sqrt{\alpha}$$

$$N_{\text{turns}} \cong 0.76\sqrt{\alpha}, \qquad \Delta V/v = (V_{\text{exit}} - V_0)/vN_{\text{turns}} \cong 4.87 \tag{20}$$

We also note that for a spiral slingatron in which the projectile accelerates in a phase-locked manner[6] the outer radius is $R \cong r(V/v)$. For the same values of projectile speed, swing speed v, and radius r, we see from Eq. (20) that the ring slingatron radius is smaller by approximately

$$R(\text{phase locked}) \cong R_{\text{ring}}(\text{phase swing})\left(1 + 1.85\Big/\sqrt{\alpha} + 1/\alpha\right) \tag{21}$$

This occurs because the projectile undergoes a swing in relative phase (Fig. 3) that causes it to spend a longer time in the accelerating phase range as it passes around the ring (or close-turns spiral) and, thus, to gain energy for several cycles around the ring. Figures 6 and 7 show some plots of formulas (20), and we next consider three examples.

Example 1: Two-Stage Machines Where Projectile Starts from Rest Relative to the Tube

Figure 5 shows a two-stage example. For single-shot operation, a projectile can be anchored inside the tube entrance of the first small spiral before the gyration is energized. In this case, the anchored projectile is simply released with a zero speed relative to

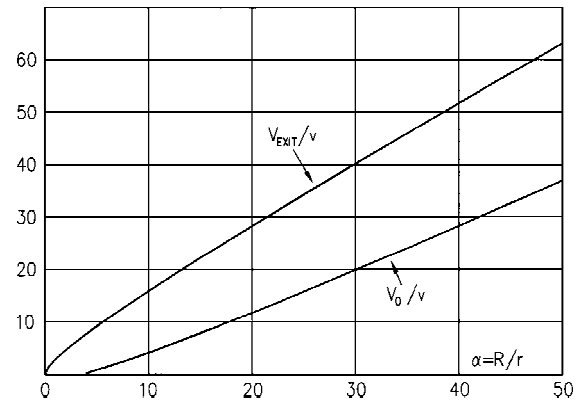

Fig. 6 Ratios V_{exit}/v and V_0/v as function of $\alpha = R/r$; injection and exit projectile velocities V_0 and V_{exit} are relative to the track.

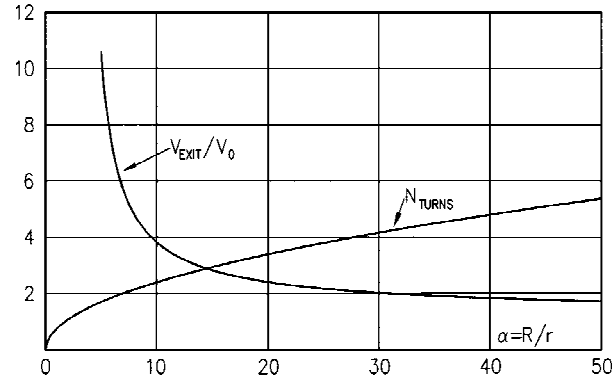

Fig. 7 (Projectile exit velocity/injection velocity) and number of cycles N_{turns} around the ring to maximum velocity, as functions of R/r.

the tube when the swing velocity $\boldsymbol{v}$ is in the half-cycle for which its centripetal acceleration has a forward component, so that the projectile is pressed back against the breechblock. After its release, the projectile continues moving with the breechblock until the swing velocity $\boldsymbol{v}$ becomes parallel to the tube ($\theta = 0$). The tube then continues around its gyration circle, but pulls back so that the projectile moves forward relative to the breechblock and starts its acceleration around the small-radius "first-stage" spiral. After reaching its maximum speed (returning to $\theta = 0$), the projectile moves on into the "second-stage" large R spiral, where it is further accelerated.

First Stage

Setting $V_0 = 0$ for the projectile speed relative to the tube at the beginning of the first stage gives, from Eq. (20),

$$\alpha = 3.42, \qquad R = 3.42r, \qquad V_{\text{lab,exit}}/v = 1 + V_{\text{exit}}/v = 7.84$$

$$N_{\text{turns}} = 1.41, \qquad n_{\text{pairs}} \cong 15(2r/L_{gap}) \tag{22}$$

where n_{pairs} is the number of swing arm pairs (Fig. 1) distributed along the first-stage spiral, and $L_{\text{gap}} \cong 2r$ is the spacing between the arm center spindles. An example for this first-stage spiral is swing speed $v = 125$ m/s and exit $V_{\text{lab,exit}} = 980$ m/s. This small radius "injection stage" can also function as an injector into a second stage.

Second Stage

The second-stage close-turns spiral (or ring) has a projectile entry speed $V_0 = 6.84v$ relative to the tube, so that from Eq. (20) it follows that

$$\alpha \cong 13.7, \qquad V_0/v \cong 6.84, \qquad V_{\text{lab,exit}}/v = 1 + V_{\text{exit}}/v \cong 21.5$$

$$N_{\text{turns}} \cong 2.8 \approx 3, \qquad n_{\text{pairs}} \cong 121(2r/L_{\text{gap}}) \tag{23}$$

For example, a swing speed $v = 125$ m/s gives $V_{\text{lab,exit}} \cong 2.68$ km/s.

Example 2: Single-Stage Machines with Finite Injection Speed Relative to Launch Tube

Consider a projectile injected with a speed $V_0 \cong 737$ m/s relative to the track into a sling orbiting with a swing speed $v = 200$ m/s, for example, a gun injection speed of 937 m/s in the laboratory frame. For this case Eq. (20) gives $\alpha \cong 9.34$ and a projectile exit speed $V_{\text{exit}} \cong 3$ km/s (3.2 km/s in the laboratory frame) achieved in $N_{\text{turns}} \cong 2.32$ turns.

Example 3: Two-Stage High-Velocity Machines

Figure 8 shows a conceptual two-stage sling in which a projectile is injected, for example, using a low-jitter gun, into the inner-turn entrance of the spiral at a phase angle $\theta(T = 0) = 0$. Injection occurs when the spiral tube entrance is aligned with (and moving away from) the gun tube. Once in the spiral launch tube, the projectile is then overtaken by a transverse displacement wave with velocity $\alpha_1 v$ that accelerates the projectile and throws it forward, so that after three turns it returns to the relative phase $\theta = 0$ at the leading edge of the wave but with much higher velocity (Fig. 3). It then passes smoothly into a larger close-turns spiral, where it is again overtaken by a much faster wave of speed $\alpha_2 v > \alpha_1 v$ and is overtaken and thrown forward to still higher speed by this second elastic collision.

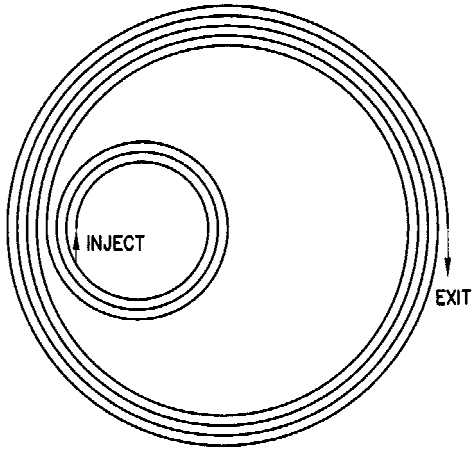

Fig. 8 Projectile accelerates through inner spiral, returns to a relative phase $\theta = 0$ with its maximum speed, and enters the larger second spiral with $\theta = 0$, where it is again overtaken and thrown forward by a faster wave.

An example of a two-stage system with gun injection into the first stage, for acceleration of projectiles to very high velocity, is as follows.

Stage 1:

$$V_{0,1}/v = 10.9, \qquad \alpha_1 = 19, \qquad V_{\text{exit},1}/v = 27, \qquad N_{\text{turns},1} = 3.31$$

Stage 2:

$$V_{0,2}/v = 27.0, \qquad \alpha_2 = 38.5, \qquad V_{\text{exit},2}/v = 50, \qquad N_{\text{turns}} = 4.72$$

If future engineering develops so that a swing speed $v = 400$ m/s becomes possible, this would give an injection speed $V_{0,1} \cong 4.4$ km/s and exit speed $V_{\text{exit},2} \cong 20$ km/s.

Note that this is based on a zero-friction model, and there is currently no experimental data for projectile sliding friction and mass loss at velocities beyond a few kilometers per second. However, in the scaling section, we present an argument that the projectile sliding friction coefficient and mass loss might decrease with increasing projectile size.

Projectile Feed Approaches

There are several ways to feed a series of projectiles into an orbiting spiral tube, and we give three concept examples. Figure 9 shows a gun injection system as used in example 3. The projectile is injected into the spiral entrance when the entrance tube is aligned with, and moving away from, the gun tube, that is, $\theta = 0$ at $t = 0$, as assumed for Eq. (13). It appears practical to meet the timing requirements with a low-jitter gun so that projectiles could be launched across a gap and reproducibly enter the tapered cone entrance of a spiral orbiting tube.

Figure 10 shows a second approach, in which an injection block executes a linear oscillation on rails.[9] It briefly comes to rest at its maximum amplitude on the right side of the rails, where it picks up a projectile at the feed block. The center piston then carries the injection block with its projectile back along the rails to the left, after which it returns and passes through its center position very close to the spiral entrance with the same velocity as the entrance. The projectile is injected during this close pass. For this injection scheme, $\theta = -\pi/2$ in Fig. 3 at injection, but can be restored to $\theta = 0$, $t = 0$, when it enters the spiral first turn by use of a short straight drift section of tube at the beginning of the spiral.

The third example (Fig. 11) shows a centrifugal feed system[9] in which a tube shaped like a crank arm extends perpendicular to the spiral plane. The lower pivot swings around the gyration circle, and the upper pivot is stationary. A projectile punched into the stationary

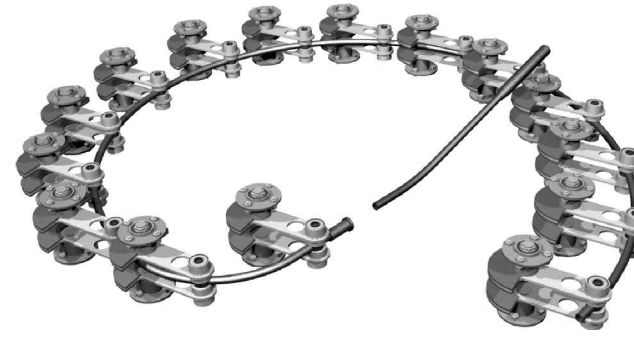

Fig. 9 Gun injection of projectiles into a gyrating spiral sling.

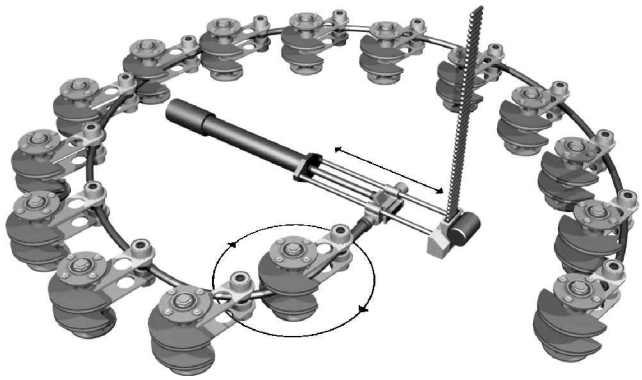

Fig. 10 Concept in which projectiles are injected from a feed block that linearly oscillates on rails and matches speed and position with the spiral entrance.

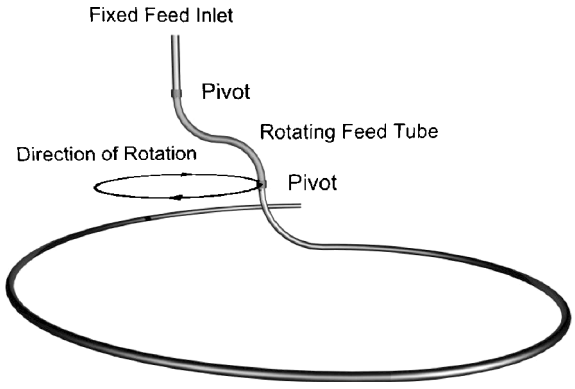

Fig. 11 Projectiles are fed into a stationary feed inlet, accelerated by centripetal force in the rotating feed tube, and then pass down into the gyrating spiral accelerator.

feed inlet is accelerated by centripetal force to swing speed v as it moves out through the tube between the pivots. It then passes down into the spiral, where it is further accelerated. This has the advantage that the entrance tube is stationary and connects continuously to the gyrating spiral, but the feed involves a small radius of curvature tube that limits the projectile length.

Scaling to Larger Geometrically Similar Slingatrons and Projectiles

Suppose a slingatron has been designed and operates successfully to accelerate projectiles of mass m to velocity V. Consider what happens if one built a geometrically similar system with the same values for the swing velocity v and projectile velocity V, that is, a system with all its spatial dimensions (including those of the projectile) multiplied by β while holding v and V constant. The mass of all components including the projectile would then increase by a multiplying factor β^3. However, the swing radius r and the ring (or spiral) radius R and swing period f^{-1} would all increase as β, so that all centrifugal accelerations would decrease as β^{-1}, and the centrifugal forces would thus increase as β^2. However, because the strength of the swing arms is proportional to their cross-sectional areas, that is, to β^2, it follows that the scaled swing arms would be mechanically viable. Note also that the bearings at the end of the arms have rated loads that are proportional to their side areas, that is, to β^2, and rated revolutions per minute proportional to β^{-1}. Finally, the impulse per unit length delivered to the launch tube, mV/R, is proportional to β^2, and the launch tube mass per unit length is similarly proportional to β^2, so that the tubes' ability to contain the projectile impulse per unit length remains the same. We see that the entire geometrically similar scaled-up sling appears mechanically viable.

A check of the lowest frequency transverse mode of a span of launch tube between neighboring swing arms shows that its frequency[6] scales as β^{-1}. Because this is the same as the swing frequency scaling, $f \propto \beta^{-1}$, resonance between the launch tube transverse modes and the swing frequency continues to be avoided for the scaled-up sling. Next we consider the two basic friction coefficients in the system.

Scaling of Rolling Friction Coefficient

The rolling friction coefficient of the roller bearings is usually expressed as $\mu_{\text{roll}} = k/r_{\text{roller}}$, where k is a constant depending on the surface quality of the rollers and race,[11] that is, μ_{roll} is proportional to β^{-1}. The machine thus dissipates its orbiting kinetic energy more slowly for larger systems.

Scaling of Projectile Sliding Friction Coefficient

Physical processes in the gas bearing involve evaporation out blowing from the low-conductivity projectile (or sabot) contact surface, high shear gas dynamics with possible turbulence driven by track asperities, thermal conduction into the track, radiation transport, and a slight tilt in the projectile due to accumulation of gas toward the rear of the projectile (Fig. 12).

To obtain a size scaling guideline, we greatly simplify the preceding picture and assume the gas film behaves like a simple laminar gas flow between surfaces in relative motion and also note that the average pressure in this film is $P = (mV^2/RA)$, which scales with system (and projectile) size as $P = \text{const}$ for a given V. The projectile friction coefficient can then be written approximately as

$$\mu_{\text{slide}} = \frac{(\text{drag/area})}{(mV^2/RA)}$$

$$= \eta_{\text{visc}} \left(\frac{\partial V}{\partial y} \right) \Big/ P \propto \frac{(P\tau_{\text{scatt}})(V/y_{\text{film}})}{P} = \frac{\tau_{\text{scatt}} V}{y_{\text{film}}} \qquad (24)$$

where we expressed the viscosity η_{visc} of the gas film in terms of the gas pressure P and the average atomic scattering time τ_{scatt} for momentum transfer collisions in the gas and y_{film} is an average thickness for the gas bearing.

We next note that the viscous drag power $\mu_{\text{slide}} F_{\perp} V$ scales as β^2/y_{film}. Also, the power lost into the hot-gas wake behind the projectile scales as $y_{\text{film}}\beta$ (β accounts for the bearing width) because the bearing gas pressure and energy density scale as a constant. Equating these two powers, that is, neglecting energy loss into the track heating, gives for the gas bearing film thickness $y_{\text{film}} \propto \beta^{1/2}$ and for the friction coefficient (24), $\mu_{\text{slide}} \propto \beta^{-1/2}$.

The projectile mass loss Δm in sliding to velocity V can be calculated by noting that $\dot{m}$ is the gas loss rate from the bearing into the wake and integrating over the acceleration time (that scales as β). The scaling estimates for similar v and V machines can then be listed as

$$y_{\text{film}} \propto \beta^{\frac{1}{2}}, \qquad \mu_{\text{slide}} \propto \beta^{-\frac{1}{2}}, \qquad (\Delta m/m)_{\text{loss}} \propto \beta^{-\frac{1}{2}} \qquad (25)$$

where we also assumed that the bearing gas temperature is a function only of velocity V for the geometrically similar constant-P family of slings. Although results (25) are based on an extremely simple model, they suggest that the projectile friction coefficient

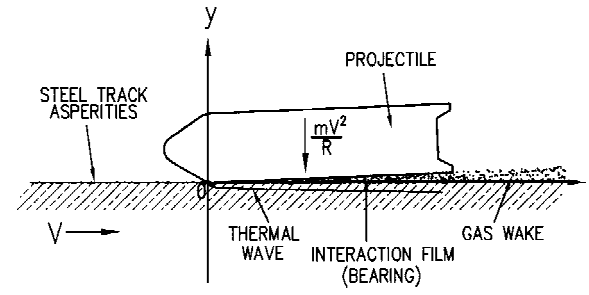

Fig. 12 Projectile shown in frame where projectile is at rest and the track slides to the right with speed V.

and total mass loss fraction for a given final velocity may decrease for increasing projectile size.

Equation (1) in Ref. 6 provides an approximate equation for the acceleration dynamics including friction, from which it follows that projectile acceleration continues for the velocity range $V < (v \sin\theta)/\mu$. Very little data are currently available for evaporation-supplied gas friction coefficients at high velocity, although μ is expected to be a function of both β and V. Experimental data[6] for small polycarbonate projectiles of mass 0.78 g gave $\mu \cong 0.02$ at 2 km/s, so that for a swing speed $v = 200$ m/s and phase angle $\theta_{\max} = 3\pi/4$, the preceding acceleration condition would be $V < 7.07$ km/s. However, if the gas film friction decreases as in results (25), that is, as $m^{-1/6}$, and we scale from the small mass value $\mu = 0.02$ for 0.74 g to the value $\mu = 0.0041$ for a 10-kg projectile, the acceleration range becomes $V < 34$ km/s. Assuming the projectile accelerating force is required to be at least twice the sliding friction force, the practical velocity limits for the above examples would become 3.5 km/s for 0.74 g and 17 km/s for 10-kg projectiles.

Conclusions

The ring and close-turns spiral mass accelerators discussed here are smaller than the phase stable machines discussed earlier. The closeness of neighboring spiral turns also allows cross struts orbiting with swing speed less than v, the same f, and radius less than r, at the ends of a few arm center spindle shafts, to assist synchronism of the orbital motion when powered up to speed. The principal issues for the slingatron concept are 1) to design and fabricate machines capable of high orbital speeds with a long statistical lifetime for the bearing assembly, together with components for projectile injection, and 2) to obtain data and physics models enabling one to minimize the sliding friction coefficient and mass loss of projectiles.

The particular design approach shown in Fig. 1 shows flat horizontal swing arms that must be spaced around the ring with gaps of length greater than L_{arm}. This design is attractive for an initial demonstrator because it would be simple to fabricate and is capable of swing speeds greater than 100 m/s. However, the launch tube segment mass that must be carried per arm determines the maximum swing speed that can be obtained with bearings that are available and can be packaged at the tube end of the arms. Both axial stacking and radial nesting of bearings at the arm ends appear useful for increasing load capacity.

For future development one could also design swing arms that are oblique to the swing plane. These could be deployed more closely around the ring,[6,9] thus, reducing the mass per arm pair that must be carried and, in turn, allowing a higher swing speed. The combination of oblique arms with possible reciprocating machinery[6] (which eliminates individual counterweights) may allow even closer spacing of swing arms and, if combined with the use of advanced materials, might lead to machines capable of swing speeds $v > 400$ m/s (corresponding to projectile gains greater than 2 km/s/turn). The value of increasing v (swing) is apparent from Eq. (20), and it also reduces the sliding distance for projectile mass loss.

Construction of a high-velocity slingatron would provide mechanical data that would be useful for further development and also data for the sliding friction and mass loss of projectiles. The "residence time" of gas evaporated from a projectile into the bearing film is longer for larger projectiles because they have a larger bearing contact area. This may result in a thicker gas film, a smaller sliding friction coefficient, and a smaller fractional mass loss from the projectile. Thus, large projectiles appear capable of surviving to much higher velocity than small projectiles. The mechanical rolling friction coefficient of the sling machinery also appears to decrease for machines of larger size.

Acknowledgments

This work was supported by the Advanced Launch Corporation. The author wishes to thank J. Chafe of Maritime Applied Physics Corporation for useful discussions and Mark Kregel of Kregel Technical Services (KTS) for useful discussions and artwork.

References

[1]Tidman, D. A., "Slingatron Mass Launchers," *Journal of Propulsion and Power*, Vol. 14, No. 4, 1998, pp. 537–544.

[2]Tidman, D. A., "A Scientific Study on Sliding Friction Related to Slingatrons," UTRON, Inc., Final Rept. U. S. Army Contract DAAD17-00-P-0710, Feb. 2001.

[3]Tidman, D. A., "The Spiral Slingatron Mass Launcher," *Space Technology and Applications International Forum-2001*, edited by M. S. El-Genk, CP-552, American Inst. of Physics, College Park, 2001.

[4]Cooper, G. R., Tidman, D. A., and Bundy, M. L., "Numerical Simulations of the Slingatron," *Journal of Propulsion and Power*, Vol.18, No. 2, 2002, pp. 338–343.

[5]Bundy, M. L., Tidman, D. A., and Cooper, G. R., "Sizing a Slingatron-Based Space Launcher," *Journal of Propulsion and Power*, Vol. 18, No. 2, 2002, pp. 330–337.

[6]Tidman, D. A., "Slingatron: A High Velocity Rapid Fire Sling," *Journal of Propulsion and Power*, Vol. 18, No. 2, 2002, pp. 322–329.

[7]Cooper, G. R., and Tidman, D. A., "Study of the Phase-Lock Phenomenon for a Circular Slingatron," *Journal of Propulsion and Power*, Vol. 18, No. 3, 2002, pp. 505–508.

[8]Tidman, D. A., "Method and Apparatus for Moving a Mass in a Spiral Track," U.S. Patent 6,014,964, Jan. 2000.

[9]Tidman, D. A., and Kregel, M. L., "Spiral Mass Launcher," U.S. Patent Application, Serial No. 10/091,025, filed 6 March 2002.

[10]Gradshteyn, I. S., and Ryzhik, I. M., *Table of Integrals, Series, and Products*, Academic Press, 1980, p. 154, p. 904.

[11]Gray, D. E. (ed.), *American Institute of Physics Handbook*, 3rd ed., McGraw–Hill, 1972, pp. 2–47.